analytical chemistry

Article

pubs.acs.org/ac

An RNA Aptamer-Based Microcantilever Sensor To Detect the Inflammatory Marker, Mouse Lipocalin-2

Lijie Zhai,[†,§,▽] Tianjiao Wang,[†,▽] Kyungho Kang,[‡] Yue Zhao,[‡] Pranav Shrotriya,[‡] and Marit Nilsen-Hamilton*[,†]

[†]Department of Biochemistry, Biophysics and Molecular Biology and [‡]Department of Mechanical Engineering, Iowa State University, Ames, Iowa 50011, United States

Supporting Information

ABSTRACT: Lipocalin-2 (Lcn2) is a biomarker for many inflammatory-based diseases, including acute kidney injury, cardiovascular stress, diabetes, and various cancers. Inflammatory transitions occur rapidly in kidney and cardiovascular disease, for which an in-line monitor could be beneficial. Microcantilever devices with aptamers as recognition elements can be effective and rapidly responsive sensors. Here, we have selected and characterized an RNA aptamer that specifically binds mouse Lcn2 (mLcn2) with a dissociation constant of 340 ± 70 nM in solution and 38 ± 22 nM when immobilized on a surface. The higher apparent affinity of the immobilized aptamer may result from its effective multivalency that decreases the off-rate. The aptamer competes with a catechol iron-siderophore, the natural ligand of mLcn2. This and the results of studies with mLcn2 mutants demonstrate that the aptamer binds to the siderophore binding pocket of the protein. A differential interferometer-based microcantilever sensor was developed with the aptamer as the recognition element in which the differential response between two adjacent cantilevers (a sensing/reference pair) is utilized to detect the binding between mLcn2 and the aptamer, ensuring that sensor response is independent of environmental influences, distance between sensing surface and detector and nonspecific binding. The system showed a detection limit of 4 nM. This novel microcantilever aptasensor has potential for development as an in-line monitoring system for mLcn2 in studies of animal models of acute diseases such as kidney and cardiac failure.

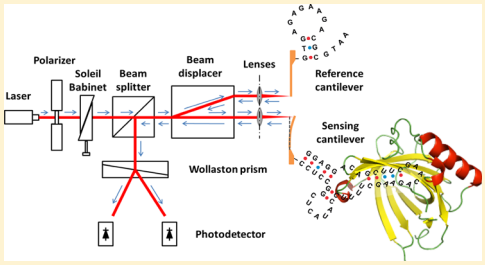

Lipocalin-2 (Lcn2) is a member of the lipocalin superfamily. Increased blood levels of the human Lcn2 (NGAL) are associated with many diseases. Lcn2 is a reliable and early indicator of acute kidney injury (AKI) and is proposed as a promising marker for AKI diagnosis and prognosis based on a meta-data analysis from clinical studies involving 19 countries and 2538 patients.[1] For monitoring acute inflammatory responses such as acute kidney injury that can occur during medical intervention, in-line monitors are most effective.

Currently Lcn2 is detected by antibody-based immunoassays, which are not readily incorporated into in-line detection systems, in part due to the instability of antibodies to repeated use at room temperature. Nucleic acids are more stable to temperature fluctuations and aptamers can be used repeatedly for real-time detection. To date, many aptamers have been selected against a broad range of targets with binding affinities comparable to monoclonal antibodies and have been incorporated into many sensor platforms.[2]

Here, we describe the selection of an RNA aptamer that specifically recognizes mouse lipocalin-2 (mLcn2) but neither the human ortholog (NGAL) nor the chicken siderophore binding lipocalin (Ex-FABP). The aptamer binding site includes the conserved iron-siderophore binding pocket of mLcn2. The mLcn2 aptamer was incorporated into a microcantilever system and demonstrated to be capable of selectively detecting mLcn2 in a homogeneous assay. The differential microcantilever sensor utilized two adjacent microcantilevers (a sensing/reference pair) to determine the mechanical deflection induced because of specific binding between the surface-immobilized aptamer and mLcn2. To ensure that sensor response was due to specific binding, only the sensing cantilever was functionalized with the aptamer and a novel differential interferometer was utilized to determine the relative deflection between the sensing and reference cantilevers. The results of these studies suggest that a microcantilever−aptamer detection system might be developed for in-line detection of mLcn2 in studies of animal models of critical human diseases.

MATERIALS AND METHODS

Reagents. The reagents used in these studies were: T4 polynucleotide kinase and RNase I (Promega), RNase T1 and DNase I (Epicenter), RNase V1, ThermoScript reverse transcriptase and TOPO XL PCR cloning kit (Life Technologies), Taq DNA polymerase (GenScript), enterokinase (EMD Chemicals), recombinant T7 RNA polymerase (prepared in the laboratory), dNTP and NTP (Thermo Fisher Scientific, Inc.), γ-^{32}P-ATP, and α-^{32}P-ATP (MP Biomedicals), $^{55}FeCl_3$ (Perkin−Elmer), 2,3-dihydroxybenzoic acid (DHBA;

Received: July 21, 2012
Accepted: September 4, 2012
Published: September 4, 2012

Sigma–Aldrich), TALON metal affinity resin (Clontech), superflow Ni-NTA resin (Qiagen), and other chemicals (Sigma–Aldrich).

All oligonucleotides (see Table S1 in the Supporting Information) were chemically synthesized with standard desalting by either the DNA Facility (Iowa State University) or Integrated DNA Technology (IDT). The 5′-thiolated oligonucleotides were synthesized with high-performance liquid chromatography (HPLC) purification by IDT.

Recombinant Proteins. The glycosylated 10xHis-mLcn2 protein, expressed by murine myeloma cell line NS0, was purchased from R&D Systems, Inc. Recombinant 6xHis-tagged wild-type mLcn2 and its mutants, human Lcn2 (hLcn2) and chicken counterpart (Ex-FABP), were expressed in *E. coli* and purified as previously described.[3] To remove the 6xHis tags, the recombinant fusion proteins were incubated with enterokinase in the buffer containing 20 mM Tris, 50 mM NaCl, 2 mM $CaCl_2$, pH 7.4 at room temperature for 24 h. The uncut proteins and His tag were removed by capture on Nickel-NTA resin. Successful cleavage was confirmed by SDS-polyacrylamide gel electrophoresis.

In Vitro Selection of Aptamers. In vitro selection of an aptamer for mLcn2 was carried out by SELEX (Systematic Evolution of Ligands by EXponential enrichment).[4] Prior to the first round of selection, a dsDNA pool was generated from a ssDNA library (oligo487) by primer extension. Reverse transcribed polymerase chain reaction (RT-PCR) amplification was used to generate DNA for subsequent selection rounds. A random RNA oligonucleotide pool was generated by in vitro transcription, using the dsDNA as template, during certain rounds of SELEX, α-^{32}P-ATP was incorporated into the transcripts to monitor the percentage of the aptamers binding to mLcn2. For each positive selection, the RNA pool was incubated with mLcn2-Talon, the nonbinding RNAs were removed by washing, then the mLcn2-bound RNAs were eluted from the resin with 150 mM imidazole, pH 7.4. The latter RNAs were reverse-transcribed and then PCR-amplified to generate the enriched pool for the next round of selection. In addition to 10 rounds of positive selection against mLcn2-Talon, negative selections were performed prior to rounds 3, 6, and 9. For each negative selection, the RNA pool was incubated with Talon resin and the nonbinding RNAs were removed by washing to provide the sample that was mixed with mLcn2-resin for the following positive selection. The enriched pool from the 10th SELEX round was cloned into the TOPO XL PCR cloning plasmid for sequencing.

Binding Affinity Measurement. A standard filter binding assay was used to determine the dissociation constant (K_d) and for the competition assays.[5] K_d values were derived from

$$B = B_{min} + \frac{(B_{max} - B_{min})[M]}{K_d + [M]}$$

where B is percentage bound of a ligand, B_{min} the minimal percentage bound of a ligand, B_{max} the maximal percentage bound of a ligand, and $[M]$ the ligand concentration. Isothermal titration calorimetry (ITC) was also used to measure the K_d value and thermodynamics of the aptamer–mLcn2 interaction at room temperature in the presence of 50 mM Tris, 150 mM NaCl, 5 mM $MgCl_2$, pH 7.4.

RNase Sensitivity Analysis. 5′-end labeling of RNAs with ^{32}P was carried out at 37 °C for 1.5 h in a 20 μL mixture of 70 mM Tris (pH 7.6 at 25 °C), 10 mM $MgCl_2$, 5 mM DTT, 1U/μL T4 polynucleotide kinase and 2 μCi/μL γ-^{32}P-ATP (6000 Ci/mmol). The labeled RNAs were purified by electrophoresis through an 8% polyacrylamide gel containing 7 M urea. The ^{32}P-labeled aptamer (2.5 nM) with varying concentrations of mLcn2 or hLcn2 in 10 μL of reaction buffer (50 mM KH_2PO_4, 150 mM NaCl, 5 mM $MgCl_2$, pH 7.4) were incubated at 23 °C for 10 min with RNase I (5×10^{-4} U/μL) or RNase V1 (1×10^{-5} U/μL). Partial alkaline hydrolysis was done in 50 μM Na_2CO_3, pH 9.0 at 95 °C for 5 min. RNase T1 digestion of the labeled aptamer was carried out in a 10-μL reaction mixture containing 0.5–1 U/μL RNase T1, 5 M urea, 350 mM sodium citrate, 0.7 mM EDTA, pH 5.0, at 50 °C for 4 min and the reaction was stopped by the addition of loading buffer to final concentrations of 47.5% formamide, 0.05% Bromophenol Blue, and 0.05% xylene cyanol FF. Samples were analyzed, after separation by electrophoresis through a 10% denaturing polyacrylamide gel containing 7 M urea, with a Typhoon 8600 Variable Model Imager (GE Healthcare).

Microcantilever Detection Assay. A differential microcantilever sensor was utilized to determine the mechanical deformation associated with aptamer–ligand binding. The sensor consisted of two microcantilevers (a sensing/reference pair), where only the sensing cantilever was functionalized with the aptamer. A novel differential interferometer (Figure 1) was used to measure the differential displacement of the sensing cantilever, with respect to the reference cantilever. A laser beam was split into two parallel beams with mutually orthogonal polarizations, using a calcite-crystal-based beam displacer. The resulting two beams were focused on the ends of the cantilever pairs and reflected beams were recombined into a single beam with the beam displacer (Figure 1). As a result, the recombined beam is an elliptically polarized beam whose two linear components have a path length difference equal to twice the differential displacement (Δl) between the cantilevers. The elliptically polarized beam was passed through a suitably oriented Wollaston prism in order to interfere the two linear components. The intensity of the interfered signal was measured to determine the path length difference between the two beams, according to the following equation:

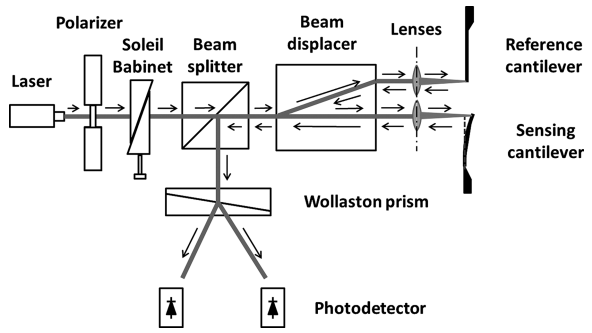

Figure 1. Schematic representation of the sensing strategy for mLcn2 detection and optical circuit of differential surface stress sensor. Laser wavelength is 635 nm. A pair of microlens arrays with lenses 240 and 900 μm in diameter, with pitches of 250 μm and 1 mm, respectively, were used to direct the beams toward the sensing/reference pair.

$$I_1 = \frac{1}{4}[I_s + I_p + 2\sqrt{I_s I_p}\cos\theta]$$

$$I_2 = \frac{1}{4}[I_s + I_p - 2\sqrt{I_s I_p}\cos\theta] \quad (1)$$

dx.doi.org/10.1021/ac3020643 | *Anal. Chem.* 2012, 84, 8763–8770

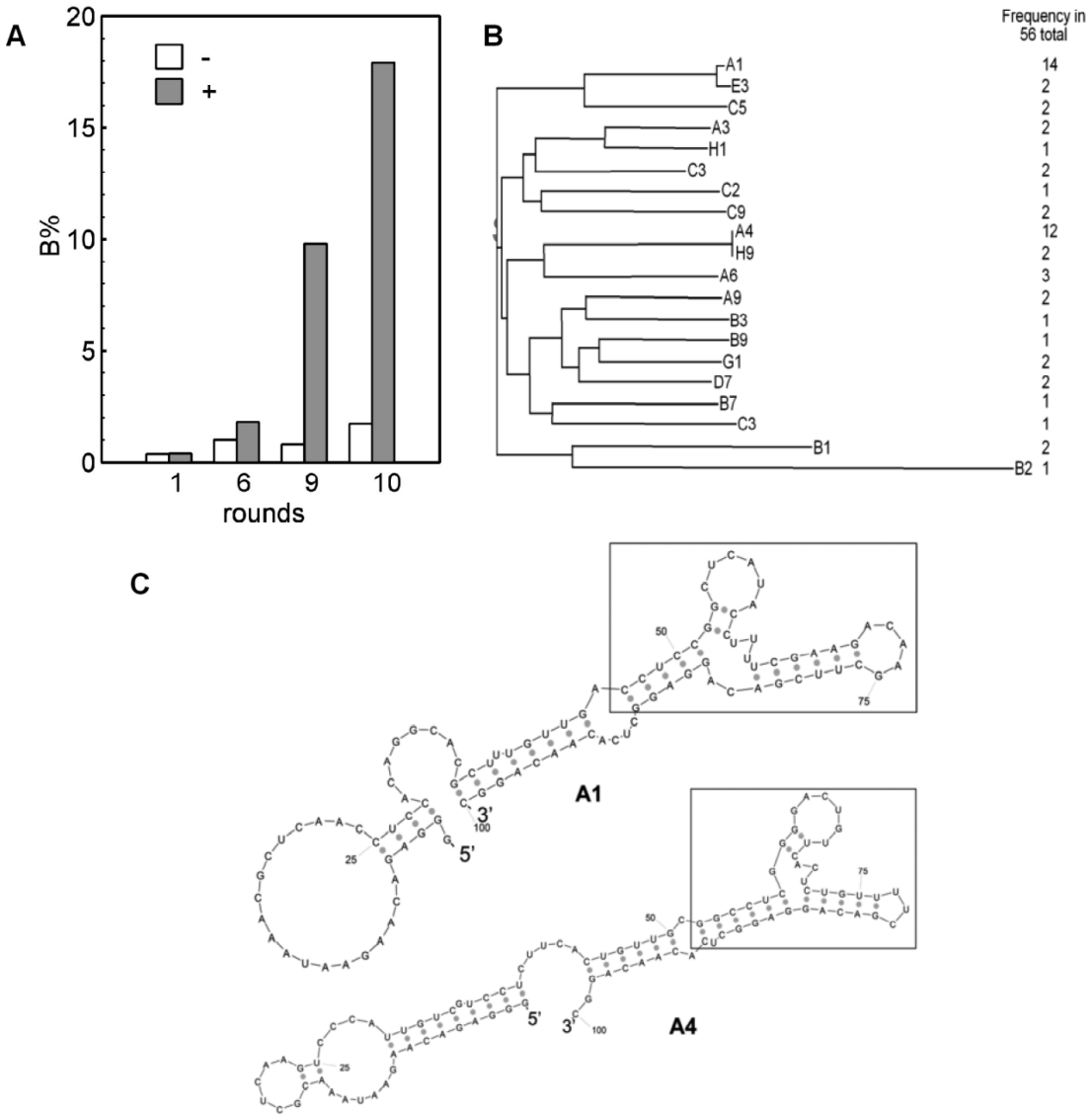

Figure 2. Selection of mLcn2 aptamers. (A) Enrichment of the mLcn2 binding RNAs during the progress of in vitro selection was monitored as the binding percentage of the RNA pool in the presence (+) and absence (−) of mLcn2 using the filter binding assay. (B) After the 10th round of SELEX, the RNAs were cloned and sequenced. Twenty one (21) different sequences were obtained from 56 clones. Sequence alignment using AlignX (VectorNTI, Invitrogen) showed that 2 of the 21 sequences (A1, A4) accounted for 25% and 21% of the population, respectively. Each sequence is denoted by a capital letter followed by Arabic numbers. The frequency of each sequence is shown at the right side of the dendrogram. (C) The secondary structures of the two dominant sequences, A1 and A4, were predicted by S-fold. The common structural element between these two candidates was identified as a three-way junction (in rectangle). Truncations of the original full length candidates were made based on this three-way junction.

where I_s (I_p) is the light intensity of the reflected beams and θ is the phase difference between the reflected beams ($\theta = 4\pi(\Delta l/\lambda$, where λ is the wavelength of the laser beam). The change of the phase difference between the linear components was monitored using the following relation:

$$\cos\theta = k\left(\frac{I_1 - I_2}{I_1 + I_2}\right)$$
$$k = (I_s + I_p)/2\sqrt{I_s I_p} \quad (2)$$

The differential displacement was utilized to determine the differential surface stress between the sensing and reference cantilevers using Stoney's formula:

$$\Delta\sigma = \left(\frac{E}{3(1-\nu)}\right)\left(\frac{t}{L}\right)^2 \Delta l \quad (3)$$

where E is the elastic modulus, ν the Poisson's ratio, L the length of the cantilevers, and t the thickness of the cantilevers. Measurement of differential surface stress ensures that the detected signal is proportional to the specific binding of ligand with aptamer on the sensing cantilever and eliminates the influence of environmental disturbances such as nonspecific binding, changes in pH, ionic strength, and especially the temperature.

In the current study, the sample cantilever was coated with 5′-thiolated oligo569, while the reference cantilever was coated with an irrelevant thiolated DNA oligonucleotide (see Table S1 in the Supporting Information). After coating, sensing and

dx.doi.org/10.1021/ac3020643 | Anal. Chem. 2012, 84, 8763−8770

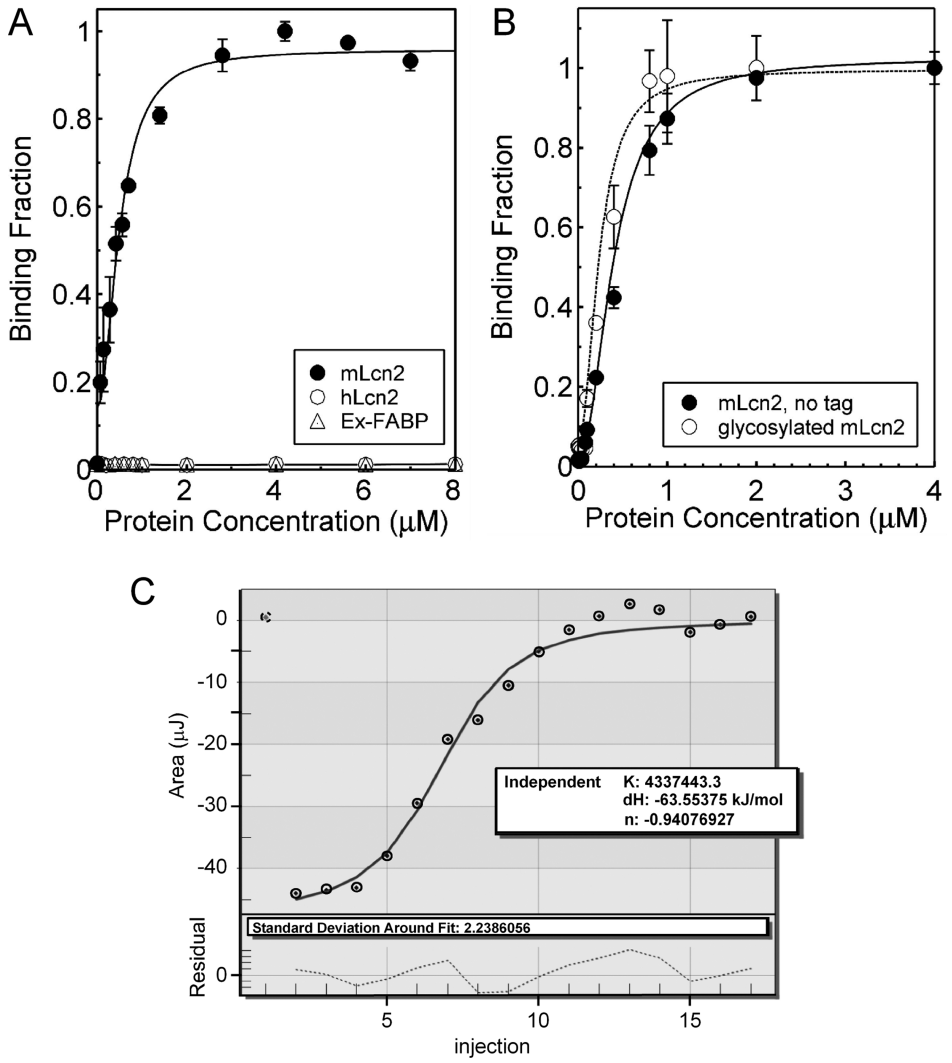

Figure 3. Specificity and affinity of the mLcn2 aptamer. (A) Lcn2 from mouse (mLcn2) was titrated against Oligo569 to determine the K_d value in more than 10 independent filter binding assays using different batches of 6xHis-mLcn2 fusion protein and oligo569. One representative dataset with a nonlinear fitting curve is shown. The binding of oligo569 to hLcn2 and Ex-FABP was determined with 3 independent filter binding assays. No detectable binding was observed for these two mutants up to 10 μM protein. For each filter binding assay, duplicates were performed to obtain the standard deviation within each assay. (B) The mLcn2 aptamer (oligo569) binds to recombinant bacterial nonglycosylated mLcn2 lacking a (●) His-tag and (○) glycosylated His-tagged mLcn2 expressed by mammalian cells. Solid line represents the nonlinear fitting curve for mLcn2 with no His-tag, and the dotted line represents the nonlinear fitting curve for the glycosylated 10xHis-mLcn2. One representative result from two independent experiments is shown for each protein. (C) The mLcn2 aptamer (oligo569) was titrated into 5 μM 6xHis-mLcn2 by ITC. The integrated area under each heat-release peak (♦) from each injection was plotted against the molar ratio of aptamer to mLcn2, and the curve was fitted with a one-site independent binding model (solid line). The first titration data point (broken circle) was omitted from the analysis. One representative result from two independent experiments is shown.

reference cantilevers were further incubated in 3 mM solution of 6-mercapto-1-hexanol for 1 h to displace any physisorbed sequences and to fill the unoccupied gold bonding sites between the immobilized receptor molecules. The differential surface stress changes were plotted against the protein concentrations, and the K_d value was calculated by the nonlinear fitting curve with the same equation as that used for K_d determination in the filter binding assay, with the B_{max} and B_{min} representing maximal and minimal surface stress changes, respectively. The limit of detection (LOD) was derived from the lowest measured signal (X_L), using the nonlinear fitting equation, with $X_L = X_{bl} + 3S_{bl}$ for which X_{bl} is the mean of the blank measurement and S_{bl} is the standard deviation of the blank measurement.[6]

RESULTS

Selection of mLcn2 Aptamers. The SELEX procedure was performed for 10 rounds, after which the mLcn2 bound RNA was found to have been enriched to 18%, from the starting 0.4%, bound to the protein (see Figure 2A). Among the 56 cloned RNAs from the 10th round, 21 aptamer candidates were identified by sequence alignment with two sequences (A1 and A4) dominating (Figure 2B). Both sequences were predicted to fold in a three-way junction (Figure 2C) and the truncated three-way junction of A1 (oligo569), which had the best affinity for mLcn2 (see Figure S1 in the Supporting Information), was further characterized.

Binding Affinity and Stoichiometry of the mLcn2 Aptamer. By filter binding and isothermal titration calorimetry (ITC) dissociation constants of 340 ± 83 nM and 210 ± 42

dx.doi.org/10.1021/ac3020643 | Anal. Chem. 2012, 84, 8763−8770

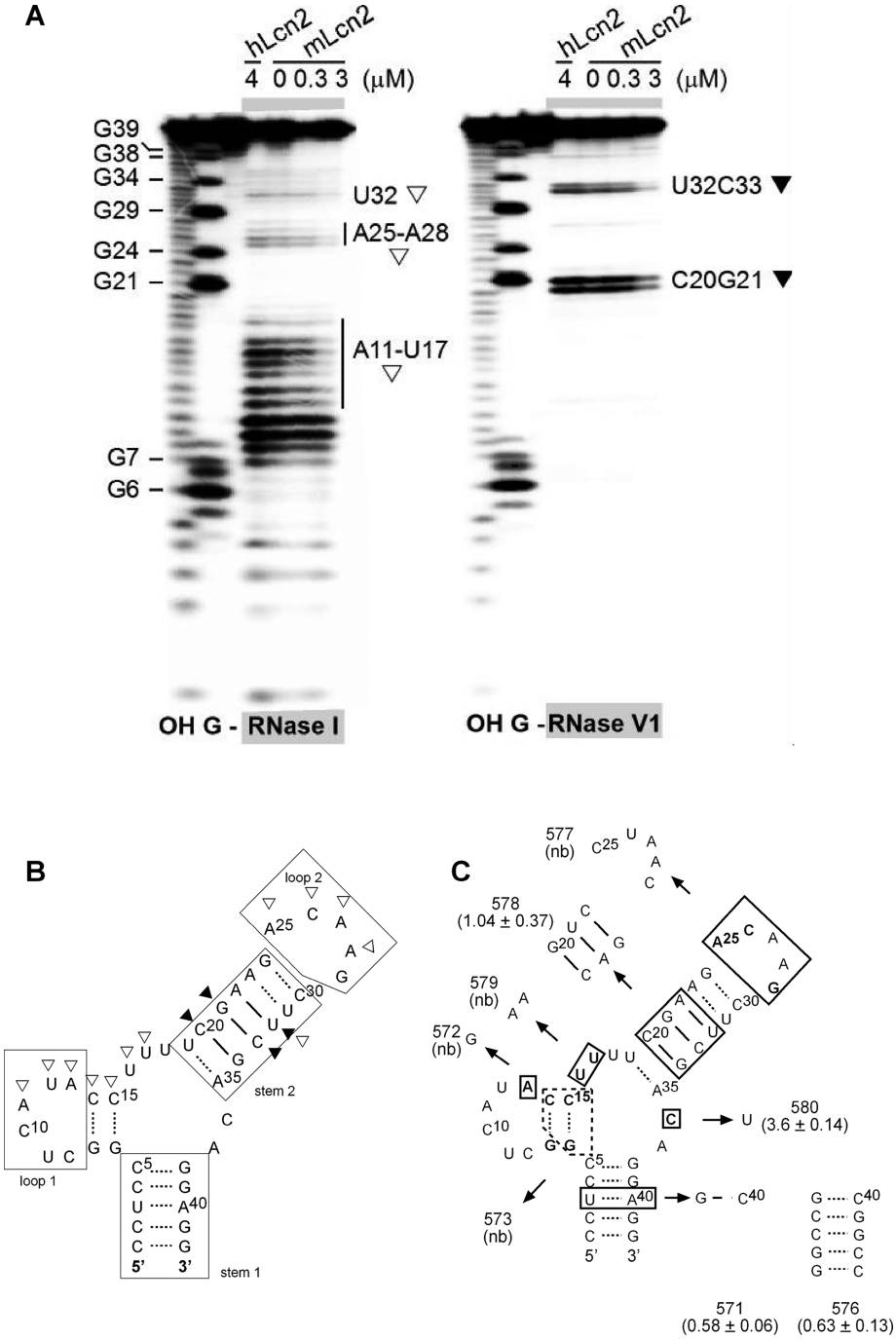

Figure 4. Identification of binding sites on the mLcn2 aptamer. (A) RNase sensitivity analysis of the mLcn2 aptamer. 2.5 nM 5′ ^{32}P-labeled oligo569 was incubated with or without 4 μM hLcn2 or mLcn2 at (0.3 and 3 μM) and subjected to digestion by RNase I (left panel) and RNase V1 (right panel). Control channels include: OH, partial alkaline hydrolysis of the aptamer; G, G ladder of the aptamer generated by partial RNase T1 digestion; −, aptamer alone with no treatment. The figure shows the results of one of at least four independent experiments. (B) Predicted secondary structure of the mLcn2 aptamer. A consensus structure from MC-Fold and S-Fold predictions includes a summary of the results for protection from cleavage by RNase I (▽) and RNase V1 (▼). Lines between the residues indicate base-pairing predicted as dynamic (dotted lines) or stable (solid lines). Possible secondary structural elements are shown in rectangles with labels. (C) Effect of variations in aptamer sequence on binding activity. A schematic representation of the mLcn2 aptamer shows the effect of varying its sequence (see Table S1 in the Supporting Information) on the affinity for mLcn2. The box with dashed-line border indicates a deletion and the boxes with solid line borders indicate substitutions. Oligonucleotide numbers are shown followed by the fold change in K_d (mean ± standard deviation (SD)), in comparison to oligo569 (average from 2−3 independent experiments). (Note that the abbreviation "nb" means no binding (K_d could not be estimated due to a lack of saturable binding by 20 μM protein.)

nM (mean ± standard deviation (SD)) were respectively determined for the binding of oligo569 to mLcn2 (see Figure 3), and the stoichiometry was 0.87 ± 0.035 (Figure 3C). The same stoichiometry was obtained by gel filtration (see Figure S3 in the Supporting Information).

dx.doi.org/10.1021/ac3020643 | Anal. Chem. 2012, 84, 8763−8770

The effect of the His tag and mLcn2 glycosylation on its interaction with the aptamer was determined by the filter binding assay. The K_d values for oligo569 binding mLcn2 without the His tag and the His-tagged glycosylated mLcn2 were 430 ± 94 nM and 380 ± 220 nM, respectively (see Figure 3B). Thus, oligo569 (aka mLcn2 aptamer) binds mLcn2 with submicromolar affinity in a manner that is affected by neither glycosylation nor the His tag.

Binding Sites and Secondary Structure of the mLcn2 Aptamer. The binding sites for mLcn2 on the aptamer were determined by RNase sensitivity analysis with hLcn2 as a negative control for mLcn2 (see Figure 4A). Nucleotides including A11−U17, A25−A28, and U32 were protected from the RNase I digestion and nucleotides including C20−G21 and U32−C33 were protected from RNase VI digestion when the aptamer was bound to mLcn2. Based on the RNase sensitivity analysis and predicted secondary structures (see Figure S4 in the Supporting Information), the most probably secondary structure of oligo569 is a three-way junction with the two loops and stem 2 involved in binding to mLcn2 (Figure 4B), which is also the most stable predicted structure. Stem 1 probably has no direct contact with mLcn2 but may stabilize the three-way junction structure.

To further confirm the proposed secondary structure and binding interactions, sequence variants of the aptamers were synthesized (see Table S1 in the Supporting Information) and tested for their affinities to mLcn2 (see Figure 4C). Deletion or substitution of the nucleosides on the two loops (oligos 572, 573, 577, 579, and 580) either abolished or dramatically decreased the aptamer binding affinity to mLcn2 (Figure 4C). By contrast, the shuffling of stem 2 (oligo578) did not change the binding affinity and addition of G·C pairs to the stem 1 (oligo571, oligo576) slightly increased the binding affinity. These affinity changes are not likely due to changes in overall secondary structure of the variants as the secondary structures predicted for these aptamer variants retained the three-way junction of the parent sequence, except that the short G·C stem near loop 1 was lost in the predicted secondary structure of oligo573, because of deletion of the CCG residues (see Figure S5 in the Supporting Information). Taken together, these results identify the key residues on the mLcn2 aptamer contributing to high affinity binding with mLcn2, as those in loops 1 (A11−U17) and 2 (A25−G29).

Identification of Binding Sites of the Aptamer on Mouse Lipocalin-2. None of the substitutions of the charged and polar surface amino acids with alanine affected the interaction of mLcn2 and aptamer. The differences in K_d were less than 4-fold for any of these substitution mutants, compared with the wild-type (WT) protein (Table 1). Larger effects on binding were observed with alanine substitutions in the calyx (see Figure 5A and Table 1). The three calyx alanine substitutions were shown via circular dichroism (CD) to have little overall effect on mLcn2 structure (see Figure S6 in the Supporting Information), which is a conclusion supported by a crystallography study of hLcn2 with double mutations that included Arg103 in hLcn2.[7] In addition, the calyx mutants were evaluated for structural integrity by gel filtration and native polyacrylamide gel electrophoresis (see Figure S7 and Table S2 in the Supporting Information). These results show that, although there are differences between the mutants and WT proteins in the gel filtration elution profiles and in their rates of travel on electrophoresis, the differences are small and do not correlate with the ability of the aptamer to bind the protein.

Table 1. Effect of Alanine Replacements of mLcn2 Residues on Aptamer Binding[a]

mutated amino acids	K_d (mean ± SD, μM)	mutation location
mLcn2	0.34 ± 0.073	wild-type
S23A_N26A	0.65 ± 0.28	surface
D41A	1.1 ± 0.16	surface
D45A_Q46A	1.1 ± 0.24	surface
T65A_E66A	0.76 ± 0.10	surface
H120A	0.72 ± 0.15	surface
R176A_K179A	0.67 ± 0.10	surface
E80A_N81A_N82A	1.5 ± 0.46	surface
E150A_N151A	0.92 ± 0.61	surface
E169A_E172A	0.82 ± 0.26	surface
D195A_Q196A_D199A	1.7 ± 0.39	surface
R103A	2.0 ± 0.75	iron−siderophore binding sites
R103A_K147A	NB[b]	iron−siderophore binding sites
R103A_K147A_K156A	NB[b]	iron−siderophore binding sites

[a]Ten (10) surface areas containing charged or polar amino acids were predicted by the homologous modeling of mLcn2 using crystallography data from human lipocalin-2 and later confirmed by the reported mLcn2 crystal structure.[14] All the tests were repeated at least four times. The binding assays of R103A_K147A and R103A_K147A_K156A were repeated six times. [b]NB = no binding.

Therefore, we conclude that the mutant protein structures are homogeneous and approximate that of the WT protein.

The three basic calyx-exposed residues bound by the aptamer are also essential for the iron−siderophore binding to hLcn2,[8] which we confirm for mLcn2 (Figure 5B). Although the K_d values for binding to the double and triple calyx mutants are decreased, compared to the WT and single calyx mutant, all titrations reached stoichiometric binding. Bovine serum albumin (BSA), when used in place of mLcn2, showed little binding of $Fe(DHBA)_3$ at saturating $Fe(DHBA)_3$ concentrations, thus ruling out the possibility that the observed stoichiometric binding of the double and triple mutants was due to nonspecific binding (see Figure S8 in the Supporting Information). Therefore, in addition to demonstrating that the calyx mutants bind $Fe(DHBA)_3$ more poorly than the WT, these results also support the conclusion that these mutants are structurally similar to the WT mLcn2. To determine if the aptamer binds mLcn2 by way of the siderophore or to the same amino acid residues as the siderophore, we tested for competition or cooperation between the aptamer and $Fe(DHBA)_3$ for binding mLcn2 and found that they compete (see Figures 5C and 5D). The competition is specific to the aptamer with no competition with $Fe(DHBA)_3$ for binding mLcn2 by an irrelevant RNA oligonucleotide (oligo258). This suggests that (i) the aptamer binding surface includes the same three basic residues in the mLcn2 calyx that form the siderophore binding site and (ii) the aptamer recognizes properly folded mLcn2.

Detection of mLcn2 Using an Aptamer-Coated Microcantilever. We have previously demonstrated that fiber-optic-based microcantilever sensors detect cocaine in a configuration with the cocaine aptamer linked to the cantilever.[9] Thiol-modified mLcn2 aptamer and an irrelevant oligonucleotide (see Table S1 in the Supporting Information) were coated on sensing and reference microcantilevers, respectively. Upon the

dx.doi.org/10.1021/ac3020643 | Anal. Chem. 2012, 84, 8763−8770

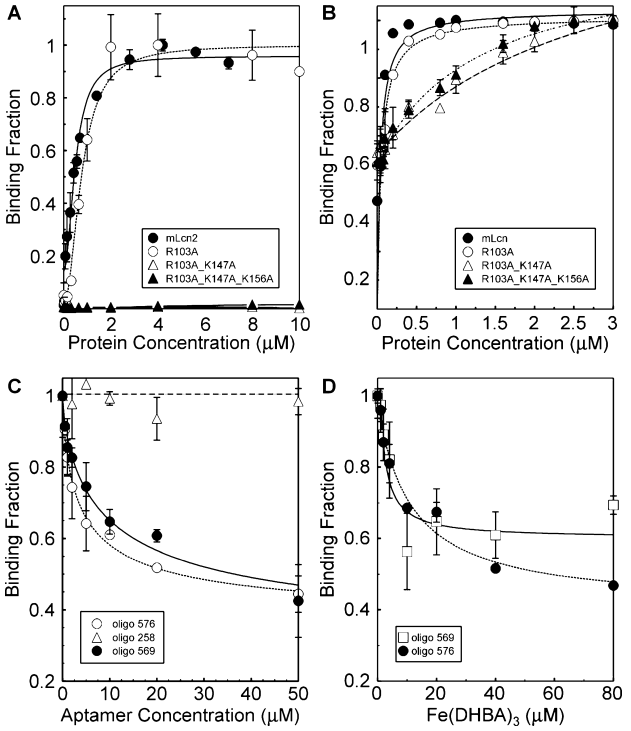

Figure 5. Identification of binding sites on mLcn2. (A) Alanine substitutions in the calyx decrease the affinity of the RNA aptamer for mLcn2. The nonlinear fitting curves are shown by the solid and dotted lines for (●) mLcn2 and (○) R103A, respectively, while the double mutants (△) and triple mutants (▲) showed no binding. One representative result is shown from at least four independent experiments for each protein. (B) Alanine substitutions in the mLcn2 calyx decrease iron−siderophore binding. Recombinant mLcn2 proteins with combinations of alanine substitutions of the amino acids Arg 103, Lys147, Lys156 were titrated against 100 nM $^{55}Fe(DHBA)_3$ ((●) mLcn2, (○) R103A, (△) R103A_K147A, and (▲) R103A_K147A_K156A). The figure shows one representative data point from at least four repeats. (C) mLcn2 aptamers compete with $Fe(DHBA)_3$ for binding to mLcn2. The fractional binding of ^{55}Fe-$(DHBA)_3$ (100 nM) bound to mLcn2 (200 nM) in the presence of various concentrations of each oligonucleotide is shown. The resulting IC_{50} values were 11 ± 2.0 μM (K_i at 2.9 ± 0.50 μM) and 5.5 ± 0.70 μM (K_i at 1.5 ± 0.20 μM) for oligo569 and oligo576, respectively. (D) $Fe(DHBA)_3$ competes with mLcn2 aptamers for binding to mLcn2. The fractional binding of ^{32}P-aptamers (2 nM oligo569 or oligo576) bound to mLcn2 (4 μM) in the presence of varying $Fe(DHBA)_3$.

addition of analytes (mLcn2 or the R103A_K147A double mutant mLcn2), the differential surface stress between these two cantilevers was recorded to measure the binding using eq 3. The binding affinity was estimated by nonlinear curve fitting of the plot of surface stress versus concentration (Figure 6). In this context, the aptamer affinity for mLcn2 was determined to be 38 ± 22 nM. This value is significantly lower than that measured for the aptamer in solution and may be due to aptamer crowding on the cantilever surface with a resulting decrease in apparent k_{off}. By fitting the experimental data using a nonlinear fitting equation, 7 mN/m was determined as the sensitivity of the surface stress measurements, and the limit of detection (LOD) for the mLcn2 concentration was estimated to be 4 nM. The microcantilever gave no significant response to the R103A_K147A mutant of mLcn2 (Figure 6) that does not bind the aptamer (Figure 5A).

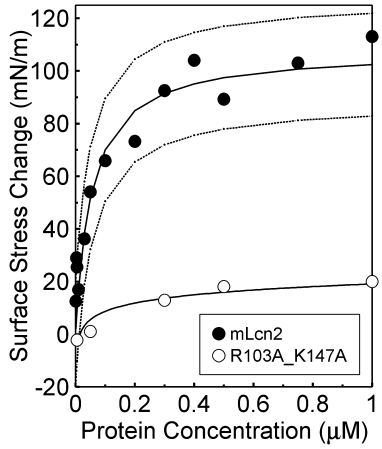

Figure 6. Surface stress values as a function of protein concentrations. Nonlinear fitting curve (solid line) was calculated from the averaged values of (●) six independent assays for mLcn2 or (○) two independent assays for mLcn2 (R103A_K147A). The two dotted lines below and above the fitting curve for mLcn2 represent the 95% confidential interval. The estimated Kd value for mLcn2 is 38 ± 22 nM.

DISCUSSION

Here, we describe the successful selection of an RNA aptamer that specifically recognizes mLcn2 with an affinity of 200−300 nM. Interestingly, when on the microcantilever, this aptamer has a 10-fold higher affinity, which could be due to a decrease in the dissociation rate of the protein from the cantilever surface on which the aptamers are highly concentrated. A concentrated surface of aptamers would increase the probability of a dissociated protein rebinding to another aptamer, compared to when both aptamer and protein are in solution. The tight molecular packing on the cantilever surface may also stabilize the aptamer structure and thereby decrease the proportion of the aptamer population that adopts alternate nonbinding structures.

With the current aptamer, the differential interferometry-based microcantilever deflection measurement allows us to detect concentrations as low as 4 nM (96 ng/mL) mLcn2. This is less sensitive than the currently available ELISA assay (LOD = 0.2 nM; R&D). However, the reported range of mLcn2 in blood ranges from 100 ng/mL (basal) to 3000 ng/mL (inflamed condition),[10] which is within the range of detection by aptamer-functionalized microcantilevers.

A common feature of aptamers is their exceedingly high specificity for the analyte against which they were selected. Consistent with this general observation, the aptamer is highly specific for the mLcn2 calyx, even though the same trilogy of amino acids is present in the same positions in the hLcn2 calyx. Sequence alignment showed that, in addition to the three iron−siderophore binding amino acids, other amino acids forming the iron−siderophore binding pockets are conserved for both human and mouse lipocalin-2 (see Figure S9 in the Supporting Information).[11] The fact that mutation of the three conserved amino acids completely eliminates binding of the aptamer to mLcn2 suggests that (i) these three amino acids form the major interaction sites of the aptamer on mLcn2 and (ii) the difference in the interaction of the aptamer with the human and mouse proteins may be because the aptamer binds to another, as yet unidentified, region on mLcn2 that is different in the

dx.doi.org/10.1021/ac3020643 | Anal. Chem. 2012, 84, 8763−8770

human Lcn2 or may be due to a dynamic aspect of their structures that is not evident in the X-ray crystallographic data.

Surface stress measurements associated with specific binding clearly demonstrate the unique advantages of the differential interferometry-based microcantilever sensor. In other state-of-the-art microcantilever-based sensors,[12] the surface stress changes are determined through optical deflectometry and the measurement resolution depends on the distance between the optical detector and the cantilever. In addition, measurements by single cantilever sensors[12b,c] are influenced by nonspecific binding and environmental disturbances such as temperature fluctuations and hydrodynamic effects. Measurement of the differential bending of the sensing cantilever, with respect to a reference cantilever, ensures that the sensor response is independent of environmental disturbances. The sensitivity of sensor measurement does not depend on the distance between the sensing surface and the detector. As a result, the surface stress sensor is amenable to miniaturization and can also include an array of sensors and be integrated with other systems on a single microelectromechanical systems device.

In conclusion, we have selected an RNA aptamer that specifically binds mLcn2 with an affinity of 210 nM in solution and 38 nM when immobilized. The RNA–protein interaction involves bases on the aptamer loop regions and the iron–siderophore binding amino acid trilogy in the calyx of the protein molecule. The aptamer is specific for the mouse over the human protein, despite the identity of amino acids to which the aptamers binds in the calyx. We have shown the potential of this aptamer as a detection probe on a microcantilever platform.

■ ASSOCIATED CONTENT

Supporting Information

Additional information as noted in text. This material is available free of charge via the Internet at http://pubs.acs.org.

■ AUTHOR INFORMATION

Corresponding Author

*Tel.: 515-294-9996. Fax: 515-294-0453. E-mail: marit@iastate.edu.

Present Address

[§]Dept. of Pediatrics, University of Chicago, Chicago, IL 60637.

Author Contributions

[∇]Co-first authors with equal contributions.

Notes

The authors declare no competing financial interest.

■ ACKNOWLEDGMENTS

We thank F. Descalzi (University of Genoa, Italy) for the pDR5 plasmid containing the Ex-FABP sequence,[13] J. Ryon for preparing the hLcn2 expression vector, E. Will for preparing the Ex-FABP expression vector, P. Palo for initial preparation of mLcn2 for SELEX experiments, and L. Bendickson for providing the data in Figure S8 in the Supporting Information and for general experimental support. L.Z. was funded by the Institute for Physical Research and Technology at Iowa State University. The U.S. Department of Energy, Office of Biological and Environmental Research through the Ames Laboratory funded the isolation and initial characterization of the aptamer. The Ames Laboratory is operated for the U.S. Department of Energy by Iowa State University, under Contract No. DE-AC02-07CH11358. The National Science Foundation Career Award (No. CMMI 0547280) funded the microcantilever studies.

■ REFERENCES

(1) Haase, M.; Bellomo, R.; Devarajan, P.; Schlattmann, P.; Haase-Fielitz, A. *Am. J. Kidney Dis.* **2009**, *54*, 1012–1024.

(2) Zhou, J.; Battig, M. R.; Wang, Y. *Anal. Bioanal. Chem.* **2010**, *398*, 2471–2480.

(3) Playford, R. J.; Belo, A.; Poulsom, R.; Fitzgerald, A. J.; Harris, K.; Pawluczyk, I.; Ryon, J.; Darby, T.; Nilsen-Hamilton, M.; Ghosh, S.; Marchbank, T. *Gastroenterology* **2006**, *131*, 809–817.

(4) Fitzwater, T.; Polisky, B. *Methods Enzymol.* **1996**, *267*, 275–301.

(5) Jhaveri, S. D.; Ellington, A. D. *Curr. Protoc. Nucleic Acid Chem.* **2001**, Unit 9.3, 9.3.1–9.3.25 (DOI: 10.1002/0471142700.nc0903s00).

(6) Taverniers, I.; Loose, M.; Bockstaele, E. *TrAC Trends Anal. Chem.* **2004**, *23*, 535–552.

(7) Abergel, R. J.; Clifton, M. C.; Pizarro, J. C.; Warner, J. A.; Shuh, D. K.; Strong, R. K.; Raymond, K. N. *J. Am. Chem. Soc.* **2008**, *130*, 11524–11534.

(8) Goetz, D. H.; Holmes, M. A.; Borregaard, N.; Bluhm, M. E.; Raymond, K. N.; Strong, R. K. *Mol. Cell* **2002**, *10*, 1033.

(9) Kang, K.; Sachan, A.; Nilsen-Hamilton, M.; Shrotriya, P. *Langmuir* **2011**, *27*, 14696–14702.

(10) Flo, T. H.; Smith, K. D.; Sato, S.; Rodriguez, D. J.; Holmes, M. A.; Strong, R. K.; Akira, S.; Aderem, A. *Nature* **2004**, *432*, 917–921.

(11) Goetz, D. H.; Willie, S. T.; Armen, R. S.; Bratt, T.; Borregaard, N.; Strong, R. K. *Biochemistry* **2000**, *39*, 1935–1941.

(12) (a) Savran, C. A.; Knudsen, S. M.; Ellington, A. D.; Manalis, S. R. *Anal. Chem.* **2004**, *76*, 3194–3198. (b) Fritz, J. *Analyst* **2008**, *133*, 855–863. (c) Godin, M.; Tabard-Cossa, V. ; Miyahara, Y.; Monga, T.; Williams, P. J.; Beaulieu, L. Y.; Lennox, R. B.; Grutter, P. *Nanotechnology* **2010**, *21*, 075501.

(13) Dozin, B.; Descalzi, F.; Briata, L.; Hayashi, M.; Gentili, C.; Hayashi, K.; Quarto, R.; Cancedda, R. *J. Biol. Chem.* **1992**, *267*, 2979–2985.

(14) Bandaranayake, A. D.; Correnti, C.; Ryu, B. Y.; Brault, M.; Strong, R. K.; Rawlings, D. J. *Nucleic Acids* **2011**, *39*, E143.